Available online at www.sciencedirect.com
ScienceDirect
Polymer 48 (2007) 664–674
polymer
www.elsevier.com/locate/polymer

Molecular dynamics simulation of hydroxyapatite–polyacrylic acid interfaces

Rahul Bhowmik, Kalpana S. Katti*, Dinesh Katti

Department of Civil Engineering, North Dakota State University, CIE 201, Fargo, ND 58105, USA

Received 27 September 2006; received in revised form 7 November 2006; accepted 8 November 2006
Available online 8 December 2006

Abstract

Polymer–hydroxyapatite (HAP) composites are widely studied as potential bone replacement materials. The HAP–polymer interfacial molecular interactions have significant role on the mechanical response of composite systems. We have used molecular dynamics (MD) simulations to evaluate the nature of these interfaces in polyacrylic acid–hydroxyapatite composites. We have obtained the parameters for monoclinic hydroxyapatite in CVFF (consistent valence force field) from the known potential energy function of apatites. Our simulations indicate that potential sites for chelation and hydrogen bond formation between HAP and polyacrylic acid (PAAc) exist. Earlier, we have synthesized in situ HAP–polymer composites wherein intimate interaction between HAP and polymer is enabled through participation of polymer during HAP mineralization. Our simulations indicate that for in situ HAP, the most favorable orientation of PAAc for attachment with HAP is along the *c*-axis of HAP aligned parallel to polymer chains. Also, binding energy for ex situ HAP composites is found to be lower as compared to that of in situ HAP.

Keywords: Polyacrylic acid; Hydroxyapatite; Molecular dynamics

1. Introduction

Hydroxyapatite (HAP) is the most stable calcium phosphate mineral in the human body and mineralizes easily at specific sites in bones and teeth [1,2]. These specific crystallographic locations are influenced by various proteins [3–5]. In general, bones and teeth are complex composite structures [6]. The commonly used advanced biomaterials for bone replacement for both implant and tissue engineering applications are often HAP–polymer nanocomposites [7–9]. Other calcium phosphates have also been investigated [7]. In order to replace bone, the mechanical properties of these nanocomposites should match with that of natural bone. The resultant mechanical properties of these nanocomposite systems depend upon several factors, e.g., selection of polymer, synthesis routes, interfacial behavior, etc. It is also known that molecular phenomenon at interfaces of these nanocomposites may well remarkably influence the resultant mechanical properties [10–12]. The interfaces between HAP and polymer could be dependent upon the synthesis route employed for HAP. Earlier, we have synthesized HAP in two different ways which referred to as in situ and ex situ HAP [8,9]. In situ HAP referred to the HAP mineralized in the presence of polymer, whereas ex situ HAP referred to HAP mineralized in the absence of polymer. Earlier we have reported that the composites fabricated with identical compositions but made using in situ or ex situ HAP have distinctly different mechanical properties [8,9] due to altered interfacial behavior. Thus, it is important to study these interfaces at molecular level for both ex situ and in situ composites which would give a better understanding of the physical properties of the nanocomposite systems. It has been observed from FTIR experiments that chelation occurs in HAP–Polyacrylic acid composites [9]. Chelation is also known as calcium bridge formation which occurs between surface calcium atoms of HAP and carboxylate groups of

* Corresponding author. Tel.: +1 701 231 9504; fax: +1 701 231 6185.
E-mail address: kalpana.katti@ndsu.edu (K.S. Katti).

0032-3861/$ - see front matter © 2006 Elsevier Ltd. All rights reserved.
doi:10.1016/j.polymer.2006.11.015

polyacrylic acid (PAAc). However, in order to get more fundamental understanding of the molecular behavior of interfaces, simulations of these interfaces are required. We have used molecular dynamics (MD) simulations to study the interfaces of HAP–PAAc composites. MD is a widely used technique for studying the molecular behavior of different species [13–17].

MD is based on Newtonian classical mechanics and uses a potential function, often called force field, to calculate the energy of a system. In order to simulate interactions between dissimilar molecular entities such as polymer and HAP, it is computationally useful to define parameters for the interacting molecular entities in a common force field. The force field is often typical to the nature of the molecule. For different atom(s) the parameters of a force field are obtained either by experimental methods such as nuclear magnetic resonance (NMR) spectroscopy or from rigorous ab initio quantum mechanics based calculations. Some of the commonly used force fields are CFF91 (consistent force field) [18–20], CVFF (consistent valence force field) [21,22], ESFF (extensible systematic force field) [23], etc. Force fields such as Amber [24,25], CHARMm [26,27], OPLS [28], and CFF91 [18–20] were optimized for simulating different proteins and/or polymers. Attempts have been made to parameterize these force fields for ion–protein/polymer interactions [29–33]. Also, efforts have been made to parameterize the above force fields for inorganic materials, e.g., Katti et al. obtained parameters for simulating clay minerals in CHARMm force field [34–36], Teppen et al. have obtained parameters for different clay minerals in CFF91 force field [37], etc. However, neither of the above force fields (or any commonly used force fields) has been parameterized for simulating HAP or interaction between HAP and polymers/proteins. Recently, a few force fields have been proposed that are applicable to HAP and that predict the structure of HAP reasonably well [38–40]. Also, it has been shown that the parameters developed for these newly proposed force fields have been used to study the interaction of HAP with water [41] and incorporation of fluoride ions in HAP [42]. On the other hand, a force field such as CVFF has parameters available for many material systems and predicts polymer structures well. To study the interactions between mineral phase and polymer phase, we have derived the parameters for the CVFF potential function (force field) from the Hauptmann potential function of apatites for monoclinic HAP [38]. Details of the procedures for deriving the force field parameters are described in our previous work on molecular interactions in clay–water system [34–36]. This potential function (Hauptmann potential) has been used recently to simulate the diffusion of (OH^-) defects in hydroxyapatite [43]. The same group has also evaluated the monoclinic to hexagonal phase transformation in hydroxyapatite using the same potential field [44].

Often vibrational spectra are derived from the molecular models. Vibrational spectra are calculated by first taking a Fourier transform of the velocity autocorrelation function (VACF) [45,46]. The VACF is calculated as follows:

$$\langle V(t)V(0)\rangle = \frac{1}{N}\sum_{i=1}^{N} V_i(t+t_0)V_i(t_0) \tag{1}$$

where $V_i(t)$ is the velocity of ith atom, N is the total number of atoms used in VACF calculations.

The vibrational spectra obtained after MD simulations are approximately comparable to infrared spectra. The experimentally obtained infrared intensity is absorbance, which is a product of density of states (DOS) and molar absorbtivity [47], whereas the intensity obtained after molecular dynamics simulations represents DOS [48]. Molar absorbtivity is directly proportional to the square of the first derivative of dipole moment ($(\mathrm{d}\mu_\mathrm{d}/\mathrm{d}x)^2$). In real molecular species, the charges on atoms are continuously changing due to which $\mathrm{d}\mu_\mathrm{d}/\mathrm{d}x$ becomes a variable and depends upon the distribution of electron clouds. In classical MD simulations, the charges on each atom of a molecular species are constant, as a result of which $\mathrm{d}\mu_\mathrm{d}/\mathrm{d}x$ becomes a constant quantity. Therefore, the intensity obtained after MD simulations is different from experimentally obtained infrared intensity.

The normal modes of vibration may be obtained by describing the potential energy of a system as a Taylor series [49,50],

$$E = E_0 + \sum_{i=1}^{3N}\left(\frac{\delta E}{\delta q_i^*}\right)_0 q_i^* + \frac{1}{2}\sum_{i,j=1}^{3N}\left(\frac{\delta^2 E}{\delta q_i^* \delta q_j^*}\right)_0 q_i^* q_j^* + \cdots \tag{2}$$

where E_0 is constant and q_i* are mass weighted coordinates, the energy scale is chosen in such a way that $E_0 = 0$. For the structure to be in equilibrium, it is necessary that force on each atom is zero, which causes second term in Eq. (2) to be zero, and leaving the following second order approximation:

$$E = \frac{1}{2}\sum_{i,j=1}^{3N}\left(\frac{\delta^2 E}{\delta q_i^* \delta q_j^*}\right)_0 q_i^* q_j^* \tag{3}$$

The above equation with Newton's equation of motion yields the following set of algebraic equations:

$$\sum_{i,j=1}^{3N}\left[\left(\frac{\delta^2 E}{\delta q_i^* \delta q_j^*}\right)_0 - \delta_{ij}\lambda'\right]A_i = 0 \tag{4}$$

where δ_{ij} is the Kronecker delta, $\lambda'^{1/2}$ is proportional to vibrational frequency, and A_i are related to relative amplitudes. Wave numbers are calculated from λ'.

The intensity obtained during vibrational calculations is directly proportional to the change in dipole moment,

$$I\alpha\left(\frac{\partial \mu_\mathrm{d}}{\partial x}\right)^2 \tag{5}$$

where, μ_d is the dipole moment between two charges and x is the displacement from equilibrium.

In this work, we report interactions between polyacrylic acid (PAAc), a nondegradable polymer used in bone biomaterials for hip implants [7] and HAP. Interaction study between HAP and PAAc was performed using the obtained parameters of HAP and available parameters of PAAc in CVFF.

2. Model construction

All the calculations were performed using the Discover_3 module of InsightII (Accelrys Software Inc.) [50] except

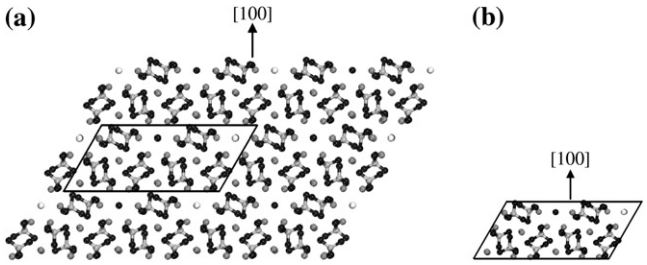

Fig. 1. Simulation cell used to get the parameters for HAP in CVFF: (a) simulation cell shown in bulk HAP; (b) simulation cell_1 (Ca = dark gray, O = black, P = light gray, H = white).

velocity autocorrelation function (VACF) and vibrational calculations after molecular dynamics simulation. These were done on Cerius2 (Accelrys Software Inc.) [50]. The Discover_3 module of InsightII includes force fields CVFF, CFF91, ESFF, etc. Parameters for monoclinic HAP are not available for these force fields.

The structural analysis of the mineral phase, HAP indicates that its stoichiometric form is monoclinic with space group $P2_1/b$ [51]. The structure of the monoclinic form of HAP is as follows: OH ions are located slightly above the *b*-glide planes, and the direction of O–H axis is parallel to the *c*-axis. The two positions of OH ions are alternately occupied. The periodicity along the *b*-axis is twice as along the *a*-axis.

For the monoclinic structure of HAP, initially two simulation cells were constructed: simulation cell_1 and simulation cell_2 for determination and validation of parameters. Here simulation cells were constructed in such a way that all the phosphate and hydroxyl ions inside the cell remain intact (Fig. 1).

The specific reasons for choice of simulation cells are described in Section 4.1.1. In order to obtain the parameters for different groups in monoclinic HAP, simulation cell_1 was used. This cell has dimensions $a = 9.421$ Å, $b = 18.84$ Å, $c = 6.881$ Å with $\alpha = 90°$, $\beta = 90°$, $\gamma = 120°$ and consists of 88 atoms. Simulation cell_2 is similar to simulation cell_1 with dimensions $a = 18.842$ Å, $b = 37.68$ Å, $c = 13.762$ Å with $\alpha = 90°$, $\beta = 90°$, $\gamma = 120°$. In simulation cell_2, 704 atoms are used to perform molecular dynamics simulations.

3. Hydroxyapatite force field parameters

3.1. Theoretical considerations

The Hauptmann potential energy function of apatites [38] is composed of an intra-atomic and an inter-atomic term,

$$E = E_{\mathrm{INTRA}} + E_{\mathrm{INTER}} \tag{7}$$

where

$$E_{\mathrm{INTER}} = \frac{1}{4\pi\varepsilon_0}\frac{q_i q_j}{r_{ij}} + w(\rho_i - \rho_j)\exp\left[\frac{R_i + R_j - r_{ij}}{\rho_i + \rho_j}\right] - \frac{C_i C_j}{r_{ij}^6} \tag{8}$$

E_{INTER} includes a Born–Mayer–Huggins (BMH) [52,53] term where r_{ij} is the distance between the *i*th and *j*th particles with charges q_i and q_j, ε_0 is the vacuum dielectric constant, ρ_i, R_i, C_i are the BMH parameters and $w = 1.1552 \times 10^{-19}$ J Å^{-1} is the standard force [54]. The intra-molecular phosphate potential E_{INTRA} is given by

$$E_{\mathrm{INTRA}} = \sum_{\mathrm{bonds}} \frac{k_r}{2}(r_{ij} - r_0)^2 + \sum_{\mathrm{angles}} \frac{k_\theta}{2}(\theta_{ijk} - \theta_0)^2 + \sum_{\mathrm{angles}} \frac{k_{\mathrm{UB}}}{2}(r_{ik} - r_0)^2 \tag{9}$$

where, k_r, k_θ and k_{UB} are the force constants, r_0 is the equilibrium distance, θ_0 is the equilibrium angle, r_{ij} is the distance between the sites *i* and *j*, r_{ik} is the distance between the sites *i* and *k*, r_0 is the equilibrium distance between sites *i* and *k*, and θ_{ijk} is the angle between the sites *i*, *j* and *k*. The third term in Eq. (9) denotes the Urey–Bradley term.

The CVFF potential energy function is given by Maple et al. [22]. We used a reduced form of CVFF potential function using a harmonic form for bond stretching term, which is useful for simulating structures consisting of organic and inorganic phases [55]. In this reduced form, the CVFF potential function is described as,

$$E = \sum_b K_b(b - b_0)^2 + \sum_\theta K_\theta(\theta - \theta_0)^2 + \sum_\phi K_\phi(1 + s\cos n\phi) + \sum_{i,j} \varepsilon_{ij}\left[\left(\frac{r_{ij}^*}{r_{ij}}\right)^{12} - 2\left(\frac{r_{ij}^*}{r_{ij}}\right)^6\right] + \sum_{ij}\frac{q_i q_j}{r_{ij}} \tag{10}$$

where K_b, K_θ and K_ϕ are force constants, b_0, θ_0 and ϕ are equilibrium bond length, equilibrium bond angle and dihedral angle, respectively, b and θ are the bond length and bond angle, r_{ij} is the distance between the *i*th and *j*th particles with charges q_i and q_j, respectively. The terms ε_{ij} and r_{ij}* determine the minimum and zero of the van der Waals term, respectively. An equivalent representation of van der Waals term (fourth term in Eq. (10)) is as follows:

$$E_{ij} = \sum\left[\frac{A_{ij}}{r_{ij}^{12}} - \frac{B_{ij}}{r_{ij}^6}\right] \tag{11}$$

where

$$A_{ij} = \varepsilon_{ij} r_{ij}^{*12} \tag{12}$$

$$B_{ij} = 2\varepsilon_{ij} r_{ij}^{*6} \tag{13}$$

In order to obtain the van der Waals parameters for CVFF from Hauptmann potential energy function, regression analysis was performed on the values obtained from BMH term of E_{INTER} for the van der Waals interactions of CVFF. In the regression analysis, energy vs. distance plot of a pair of atoms is obtained by using BMH equation which is fitted to van der Waals term of CVFF. van der Waals parameters thus obtained

Table 1
Parameters of van der Waals term in CVFF

	A_{ii}	B_{ii}
Ca	198968.2288	307.2698
H	0.0023	0.0003
O(H)	358704.8809	409.7767
O(P)	609768.2770	784.0094
P	12532927.1400	6987.9390

are for homonuclear interactions (Table 1). The heteronuclear interactions are computed from geometric averages given by:

$$A_{ij} = \sqrt{A_{ii}A_{jj}} \tag{14}$$

$$B_{ij} = \sqrt{B_{ii}B_{jj}} \tag{15}$$

A new restrain ''tether'' type term is introduced in the CVFF. This term effectively forces all the selected atoms in their original positions. The Hauptmann potential uses Urey–Bradley term between neighboring oxygens bonded to phosphorous in phosphate tetrahedron. Thus the restrain term may be considered as a way to compensate for Urey–Bradley term since we have used restrain term on oxygens bonded to phosphorous atom. The tether term is given by (used in Discover_3 module [50]):

$$E_{\text{restrain}} = \sum_{\text{bonds}} \alpha k\left(X_{ij} - X_0\right)^2 \tag{16}$$

where k is the force constant, X_0 is the initial internal (bond length, angle, etc.), α is the scaling factor and X_{ij} is the final internal. We used a scaling factor of 1 in our calculations and bond length was used for initial and final internal. The final potential energy function for CVFF is thus given by,

$$E = \sum_b K_b(b-b_0)^2 + \sum_\theta K_\theta(\theta-\theta_0)^2 + \sum_\phi K_\phi(1+s\cos n\phi) + \sum_{i,j}\varepsilon_{ij}\left[\left(\frac{r_{ij}^*}{r_{ij}}\right)^{12} - 2\left(\frac{r_{ij}^*}{r_{ij}}\right)^{6}\right] + \sum_{ij}\frac{q_iq_j}{r_{ij}} + E_{\text{restrain}} \tag{17}$$

Bonded parameters are the parameters for the bond stretching term, angle bending term and the dihedral term. According to Eq. (17), the bonded parameters for the bond stretching term are K_b and b_0, the bonded parameters for the angle bending term are K_θ and θ_0, and the bonded parameters for the dihedral term are K_ϕ, ϕ, and n. In monoclinic HAP, the P–O bond length and O–P–O bond angle of phosphate tetrahedron ranges from 1.53 Å to 1.54 Å and 106.68°–112.05°, respectively [56]. From the parameters for CVFF database, it is observed that equilibrium bond length between a phosphorous atom and ''carbonyl oxygen'' atom is 1.53 Å (here the carbonyl oxygen used is of the atom type, i.e., the name of oxygen atom given for a particular chemical environment) and the equilibrium bond angle corresponding to O–P–O is 109.5°. This equilibrium bond length and bond angle is close to that observed in monoclinic HAP. For this reason, this equilibrium length and angle is used in all calculations. Similarly, oxygen and hydrogen atom types in OH group of monoclinic HAP are taken as oxygen and hydrogen in hydroxyl group, respectively, with equilibrium bond length of 0.96 Å.

The second derivative of potential energy is often called as the force constant between sites i and j. It is clear from Eq. (4) that the band obtained at a particular wave number during vibrational calculations depends upon force constants between sites i and j. Hence, the bending force constant and stretching force constant of O–P–O and P–O were chosen in such a way that the vibrational mode of P–O results at 1050 cm^{-1} as observed experimentally [55]. Similarly, stretching force constant value for O–H was chosen so that the stretching vibrational mode results at 3672 cm^{-1} [57]. Also, the values of force constants were chosen so that the ratio of these two intensities is equal to 2.8, since the experimentally obtained ratio of intensities of P–O stretching and O–H stretching is 2.8 [58]. With this methodology, the values of stretching force constants for P–O and O–H are found to be 254.00 kcal mol^{-1} $Å^{-2}$ and 524.34 kcal mol^{-1} $Å^{-2}$, respectively, and the bending force constant for O–P–O to be 6.83 kcal mol^{-1} deg^{-2}. The above values are obtained by using simulation cell_1. Simulation cell_1 was first minimized until the values of energy derivatives were less than 0.001 kcal mol^{-1} $Å^{-1}$. The minimized cell was used for vibrational calculations. Further details of the simulation cells are described in the following section.

3.2. Simulation details

Simulation cell_1 and simulation cell_2 were first minimized using periodic boundary conditions. The periodic boundary conditions used for simulation cell_1 and simulation cell_2 were 9.421 Å × 18.843 Å × 6.881 Å with $\alpha = 90°$, $\beta = 90°$ and $\gamma = 120°$ and 18.842 Å × 37.686 Å × 13.762 Å with $\alpha = 90°$, $\beta = 90°$ and $\gamma = 120°$, respectively. The non-bonded interactions were calculated by Ewald summation method [59]. For simulation cell_1 minimization was done using steepest descent method followed by conjugate gradient method and finally with truncated Newton–Raphson method with convergence from initial 1000 kcal mol^{-1} $Å^{-1}$ to 0.001 kcal mol^{-1} $Å^{-1}$. Steepest descent method followed by conjugate gradient method with convergence from 1000 kcal mol^{-1} $Å^{-1}$ to 0.001 kcal mol^{-1} $Å^{-1}$ was used for simulation cell_2. Lattice constants and different atomic distances were compared with experiments after conducting molecular dynamics simulations for simulation cell_2 in isothermal–isobaric (NPT) ensemble for a total time of 50 ps in the temperature range from 73 K to 1273 K at 1 bar of pressure using Andersen method [60]. Canonical (NVT) ensemble was used to obtain vibrational spectra at 300 K. The vibrational spectra after MD simulation were obtained by Fourier transform of velocity autocorrelation function. The Newton's atomic equations of motions during MD simulations were integrated numerically using the Verlet leapfrog algorithm.

3.3. Parameter validation

The interaction energy between HAP and PAAc can be represented as follows:

$$E_{\text{int, HAP–PAAc}} = E_{\text{HAP}} + E_{\text{PAAc}} - E_{\text{HAP–PAAc}} \quad (6)$$

where $E_{\text{HAP–PAAc}}$ is the energy after minimizing the composite structure, E_{HAP} is the energy of the same composite structure after removing PAAc molecule and E_{PAAc} is the energy of composite structure after removing HAP molecule. Further, E_{HAP} and E_{PAAc} are the energies of HAP and PAAc, respectively, without minimizing the composite structure. The binding energy, $E_{\text{bind, HAP–PAAc}}$ is negative of interaction energy, $E_{\text{int, HAP–PAAc}}$. Higher value of binding energy implies stronger interactions or attachments.

The van der Waals parameters obtained using regression analysis on the values obtained from BMH term of E_{INTER} for the van der Waals interactions of CVFF are shown in Table 1. The bonded parameters and the charges which were used for the simulations are shown in Tables 2 and 3, respectively. Minimization of the simulation cell of monoclinic HAP was performed. It was found that force constant value of 500 kcal mol^{-1} Å^{-2} in restrain energy term, results in a good agreement with experiments in terms of lattice constants, atomic distances and the vibrational spectrum.

Molecular dynamics simulations were performed at different temperatures in a range between 73 K and 1273 K. The unit cell parameters were compared with experimental results [61] at different temperatures and are shown in Table 4 (the experimental results are the unit cell parameters at different temperatures obtained from XRD and thermal coefficient data). The observed deviations of unit cell parameters from experiments are from 0.14% to 1.90%. The deviations are less at room and at low temperatures. However, the deviations are more at high temperature (particularly at 1273 K) (in the range of 1.9%). The simulated bond lengths and angles at 300 K are also compared with experiments and are shown in Table 5 and Fig. 2. These show that different bond lengths and angles at 300 K agree well with experiments. These comparison of simulated model with experiments shows that the proposed model is good in predicting the properties of HAP and its interactions with various molecules at room temperature. However, more accurate representation of parameters is needed in order to predict the different phenomena of HAP at high temperature.

Table 2
Bonded parameters of CVFF

Bonded atoms	Bonded parameters
P–O	$K_b = 254.00$ kcal mol^{-1} Å^{-2}, $b_0 = 1.53$ Å
O–P–O	$K_b = 6.83$ kcal mol^{-1} deg^{-2}, $\theta_0 = 109.5°$
O–H	$K_b = 524.34$ kcal mol^{-1} Å^{-2}, $b_0 = 0.96$ Å

As the interactions between PO_4^{-3} and Ca^{+2} ions are mainly non-bonded type [62] (electrostatic and van der Waals), therefore the dihedral term is not considered for the present model. Same applies for the pairs OH^-, Ca^{+2} and OH^-, PO_4^{-3}.

Table 3
Partial atomic charges of different atoms of HAP used for the calculations (adapted from the Ref. [38])

Atom	Charge
Ca	+2.0
H	+0.6
O(H)	−1.6
O(P)	−1.4
P	+2.6

Table 5
Comparison of inter-atomic distances (Å) between experimental [58] and simulated model

	Experimental	Simulated
Ca(3)–Ca(4)	3.99	4.09
Ca(3)–Ca(5)	4.12	4.14
Ca(4)–Ca(5)	4.07	3.98
Ca(3)–O(4)	2.32	2.33
Ca(4)–O(4)	2.48	2.48
Ca(5)–O(4)	2.37	2.34

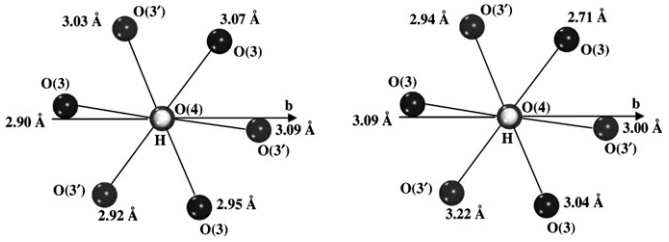

Fig. 2. Comparison of distances between hydroxyl H and O(3)s of (a) experimental [56] and (b) simulated models (O = black, H = white).

Table 4
Unit cell parameters of experimental [61] and simulation at different temperatures (% difference in lattice constant as compared to that obtained from experiments)

	a (Å)	b (Å)	c (Å)	α (°)	β (°)	γ (°)	T (K)
Expt.	9.377	18.754	6.881	90.0	90.0	120.0	73
Sim.	9.363 (+0.14)	18.727 (+0.14)	6.838 (+0.62)	90.0	90.0	120.0	
Expt.	9.404	18.808	6.901	90.0	90.0	120.0	300
Sim.	9.368 (+0.38)	18.737 (+0.37)	6.842 (+0.85)	90.0	90.0	120.0	
Expt.	9.441	18.882	6.928	90.0	90.0	120.0	600
Sim.	9.372 (+0.73)	18.746 (+0.72)	6.845 (+1.19)	90.0	90.0	120.0	
Expt.	9.556	19.111	6.940	90.0	90.0	120.0	1273
Sim.	9.374 (+1.90)	18.750 (+1.88)	6.847 (+1.34)	90.0	90.0	120.0	

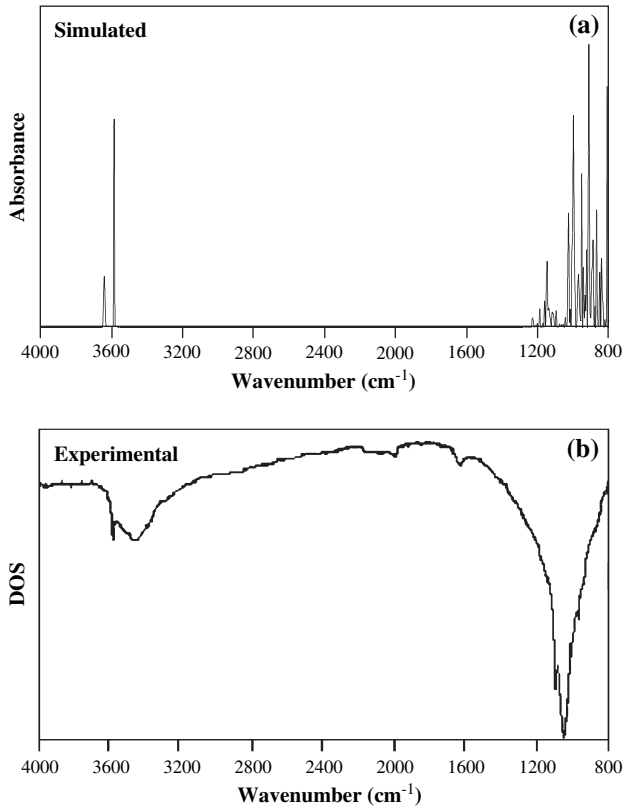

Fig. 3. (a) Computationally obtained vibrational spectra of monoclinic hydroxyapatite at 300 K. (b) Experimentally obtained vibrational spectra (adapted from Ref. [58]).

Vibration calculations were performed after doing MD simulation at 300 K using NVT ensemble. Simulated spectra show good agreement with experiments in terms of band position as shown in Fig. 3.

4. HAP–polyacrylic acid interaction study

4.1. HAP–polyacrylic acid model building

4.1.1. HAP model for interaction study

The phosphate and hydroxyl ions in HAP act as polyanions [62], therefore in simulation cells, the phosphate tetrahedron and hydroxyl ions were kept intact, as shown in Fig. 1. Surface simulations were done by creating surfaces by increasing any one of the axes *a*, *b* or *c* of the simulation cell (in this way, all the surfaces will have intact phosphate and/or hydroxyl ions). The surface generated with simulation cell_1 is dipolar. It has been shown that for such surfaces (dipolar) energy diverges with increasing crystal size [63]. The surfaces (100), (010) and (001) were made non-dipolar by removing half of the surface calcium atoms from one surface to its opposite surface resulting in 50% vacancies (as shown in Fig. 4(b), (d), and (f)). This procedure was done in accordance with Tasker et al. [64], wherein it was shown that dipolar surface can be made non-dipolar by removing half of the surface ions from a surface layer to its bottom, creating a surface with partial vacancies of ions.

4.1.2. PAAc model and charge calculations

Ab initio calculations were performed to determine the charges on each atom of PAAc using a four monomer model of PAAc. This model was first minimized using HF/6-31

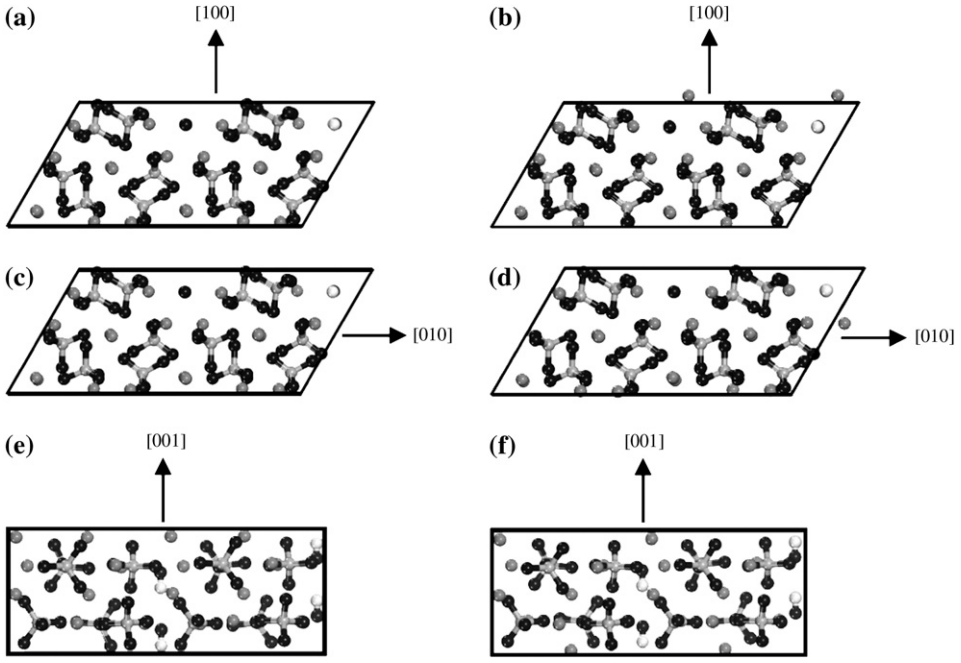

Fig. 4. Simulation cells of HAP whose surfaces were made non-dipolar by removing 50% calcium atoms from one surface to its opposite surface: (a) dipolar (100) surface (b) non-dipolar (100) surface (c) dipolar (010) surface (d) non-dipolar (010) surface (e) dipolar (001) surface (f) non-dipolar (001) surface (Ca = dark gray, O = black, P = light gray, H = white).

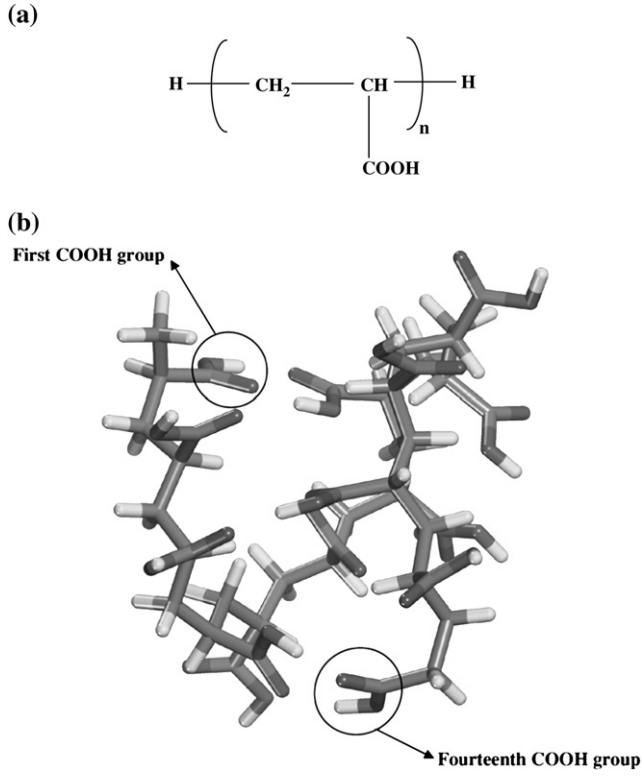

Fig. 5. (a) Structure of polyacrylic acid (where n is the number of monomers) and (b) model of PAAc used for interaction study. Here the numbering of COOH group is shown (C = light gray, H = white, O = dark gray).

G**, then the atom centered charges were calculated by Merz–Singh–Kollman method [65] using B3LYP/cc-pVQZ electric potential. All the ab initio calculations were performed using Gaussian 03 [66]. It was found that the charges on equivalent atoms (e.g., ''carbonyl carbon'') have approximately same charges. Hence we used average charges on these atoms, since in MD calculations equivalent atoms should have same charges that are constant with respect to conformational changes [67]. All other parameters for PAAc used were default values from CVFF potential function.

For interaction study with different HAP surfaces, 14 monomers of PAAc were used (Fig. 5(b)). Ten different models of PAAc were constructed each with 14 monomers. Each of the models were first minimized and then MD simulations were performed for 50 ps at 300 K. Temperature was increased from 300 K to 500 K in steps of 50 K. For each step of temperature increment, MD simulations were performed. Finally, each of PAAc chains was minimized. The PAAc chain with lowest energy was used for interaction study. Here, minimization was done using conjugate gradient method with a gradient of 0.001 kcal mol^{-1} $Å^{-1}$. Canonical (NVT) ensemble was used in MD simulations where Verlet leapfrog algorithm was used for integrating the Newton equations.

4.1.3. Building surfaces of HAP and composite structures

Three simulation cells, simulation cell_3, simulation cell_4 and simulation cell_5 of HAP were used for surface simulations and interaction study. Dimensions of simulation cell_3

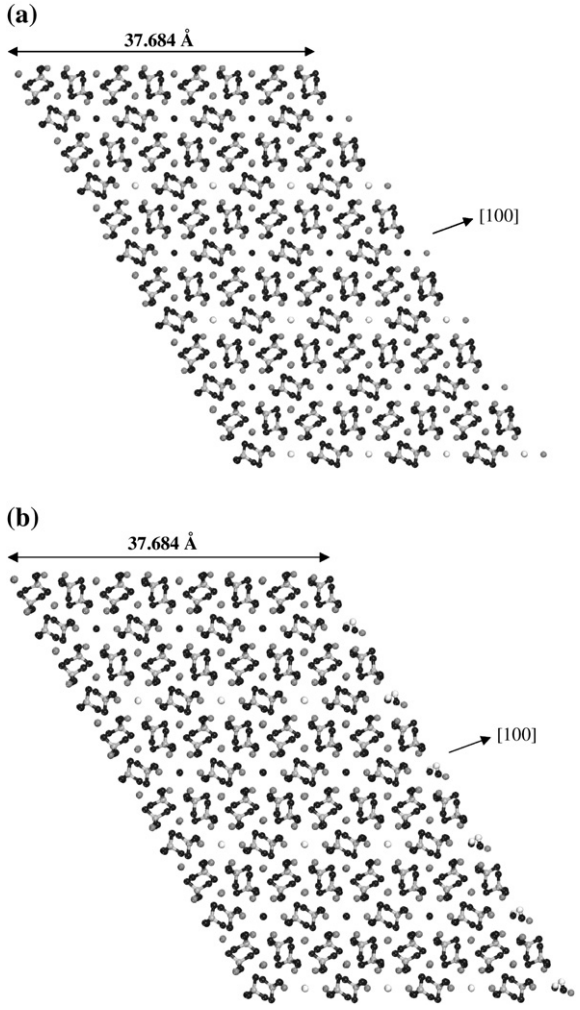

Fig. 6. (a) Unrelaxed and (b) relaxed model of HAP (simulation cell_3) where relaxed (100) and $(\bar{1}00)$ surfaces have been used for interaction with PAAc (Ca = dark gray, O = black, P = light gray, H = white).

and simulation cell_4 were $a = 37.684$ Å, $b = 56.52$ Å, $c = 20.643$ Å with $\alpha = 90°$, $\beta = 90°$, $\gamma = 120°$. Both the simulation cells were taken as 36 cells of simulation cell_1 ($4a \times 3b \times 3c$). The dimensions of simulation cell_5 were $a = 18.842$ Å, $b = 56.52$ Å, $c = 41.286$ Å with $\alpha = 90°$, $\beta = 90°$, $\gamma = 120°$, also made using 36 cells of simulation cell_1 ($2a \times 3b \times 6c$). For surface simulation, a-, b-, and c-axes of simulation cell_3, simulation cell_4, and simulation cell_5 were increased to 137.684 Å, 172 Å, and 141.286 Å, respectively. The surface of simulation cell_3, simulation cell_4, and simulation cell_5 is polar equivalent to surfaces shown in Fig. 4(c), (d), and (f). Thus the 'thick slabs' of HAP with dimensions 37.684 Å, 48.947 Å and, 41.286 Å were created for simulation cell_3, simulation cell_4, and simulation cell_5, respectively, with 3D periodic boundary conditions. In all these cases, the surfaces were separated from its image by 100 Å. A similar type of approach has been taken in literature [16,68,69] where pseudo 2D boundary conditions were constructed from 3D boundary conditions.

For interaction study with PAAc, 14 monomers were placed at all the six locations, two for each simulation cell (e.g., for

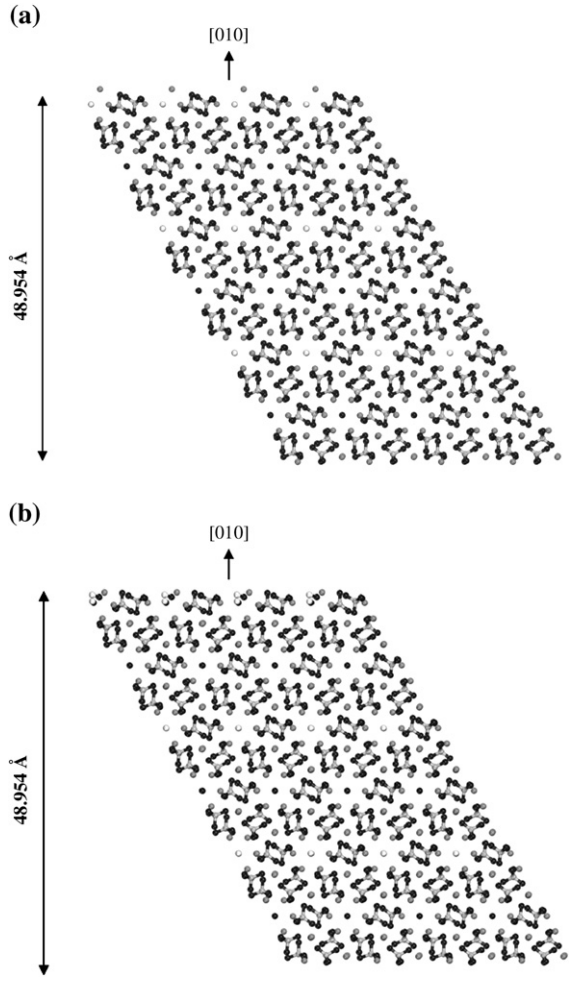

Fig. 7. (a) Unrelaxed and (b) relaxed model of HAP (simulation cell_4) where relaxed (010) and $(0\bar{1}0)$ surfaces have been used for interaction with PAAc (Ca = dark gray, O = black, P = light gray, H = white).

simulation cell_3, with planes (100) and $(\bar{1}00)$). Before doing the interaction study by MD simulations, first all the models and subsequently their surfaces were relaxed and lastly all the composite structures were minimized with 14 monomers of PAAc. Further, MD simulations were performed for 50 ps with time step of 1 fs in canonical (NVT) ensemble. Here, again Verlet leapfrog algorithm was used for integration of Newton's atomic equations. All the minimizations were done using conjugate gradient method with final convergence of 0.001 kcal mol^{-1} $Å^{-1}$. For electrostatic interactions, Ewald summation method was used. Cut off distance of 10 Å was used for van der Waals energy.

4.1.4. Interaction parameters for HAP–polymer

The CVFF also has van der Waals parameters for ion/polymer interactions. To validate our parameters for ion–polymer interactions, we compared the van der Waals interaction energy first with the obtained parameters and then with the default parameters in CVFF. This is performed by comparing each pair of atoms involving atoms of hydroxyapatite and atoms of polymer. The parameters A_{ij} and B_{ij} in Eqs. (14) and (15) are obtained by referring to '*i*' as atoms of HAP and '*j*' as atoms of polymer. The A_{ij} and B_{ij} are thus obtained. On comparing the van der Waals energy for each pairs of atoms we find that a good match is obtained for the interactions between various ions of hydroxyapatite and atoms of polyacrylic acid.

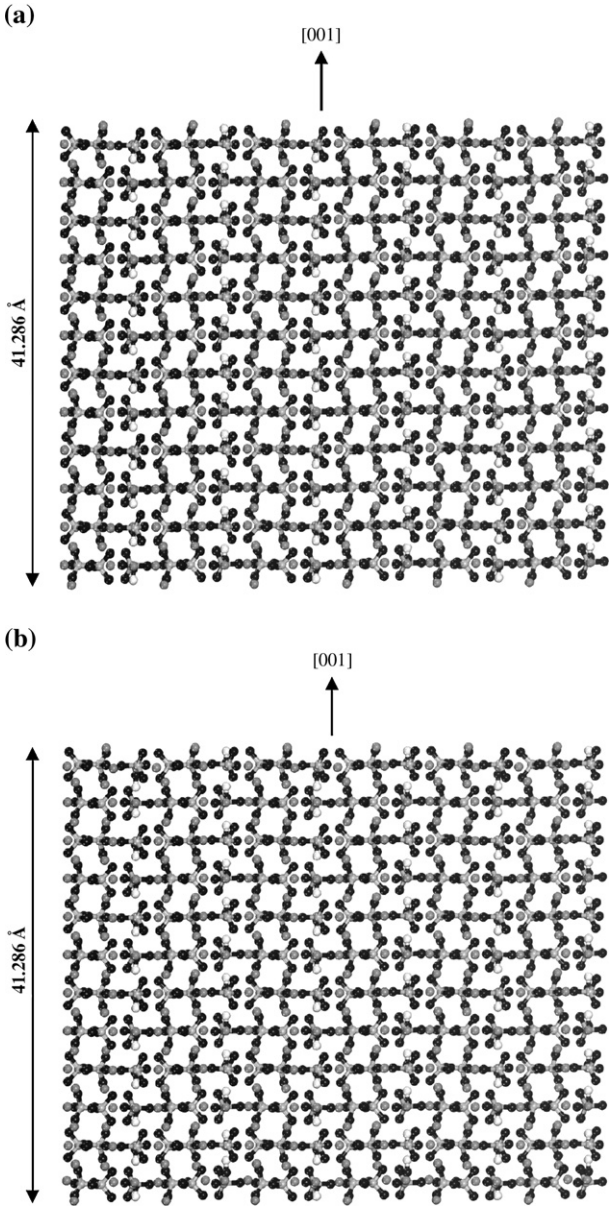

Fig. 8. (a) Unrelaxed and (b) relaxed model of HAP (simulation cell_5) where relaxed (001) and $(00\bar{1})$ surfaces have been used for interaction with PAAc (Ca = dark gray, O = black, P = light gray, H = white).

5. Results and discussion

Figs. 6–8 show the unrelaxed and relaxed surfaces of simulation cell_3, simulation cell_4 and simulation cell_5, respectively. These figures also show the thickness of HAP used in the interaction study. As seen, the relaxed surfaces terminated with OH^- ions (surfaces (100) and (010)) are more

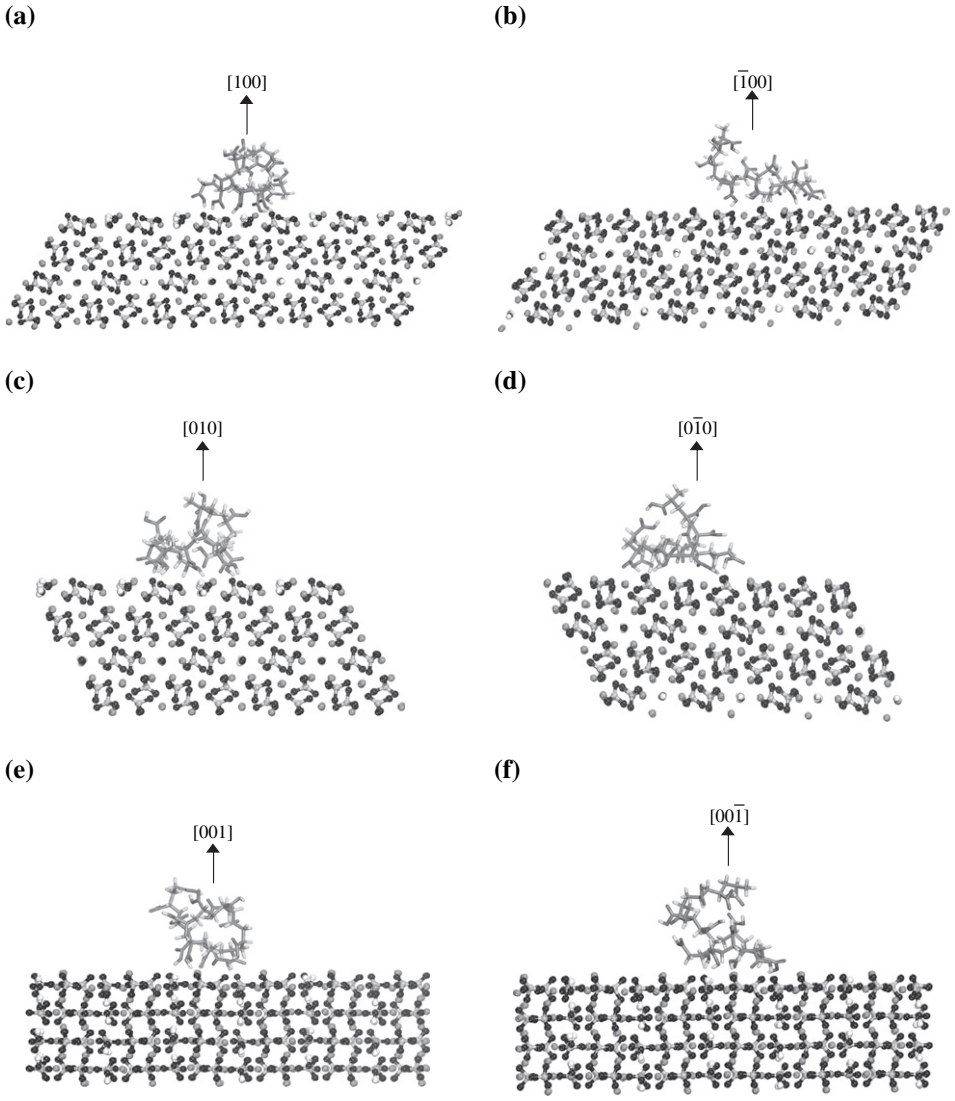

Fig. 9. Models of composite structures after MD simulations in which PAAc (shown in Fig. 5(b)) is interacting with different non-dipolar HAP surfaces. Here the relaxed HAP surfaces, which are shown in Figs. 6–8 were used. (HAP is shown in "ball and stick" model whereas PAAc is shown as "stick" model.)

distorted as compared to surfaces terminated only with Ca^{+2} or oxygen atoms of PO_4^{-3} (surface (001)) (Fig. 9).

For interaction study, PAAc chain comprising of 14 monomers was placed at six different locations around HAP separately, two for each simulation cell, e.g., PAAc was kept in the close proximity of surfaces (100) and $(\bar{1}00)$ for simulation cell_3. For each location, the composite structure was first minimized. The binding energy obtained for all the locations after minimization is shown in Table 6. It can be observed that the binding energy is highest when the polymer is attached to the (100) or $(\bar{1}00)$ surface, i.e., interactions of PAAc with these surfaces are the highest as compared to rest of the surfaces. Thus, if the surfaces which were analyzed here were available then PAAc molecules would prefer to attach to (100) or $(\bar{1}00)$ surface of HAP. It was previously observed that the most dominant surface in apatite is (001) [70,71], thus if composites are made with HAP (ex situ HAP composites) then the most probable surface on which PAAc molecules attach would be (001) or $(00\bar{1})$ surface. But in the case of in situ HAP, where HAP mineralizes on specific sites of PAAc, (100) or $(\bar{1}00)$ surfaces of HAP are more likely to form over those specific sites of PAAc.

MD simulations were performed on all the simulation cells with PAAc. After MD simulations, all the surfaces show some potential sites for hydrogen bond (H-bond) and chelation (calcium bridge) formation. Schematic representation of H-bond

Table 6
Binding energies between HAP and PAAc at different surfaces

Surface	$E_{bind,HAP-PAAc}$ (kcal mol^{-1})
(100)	969.58
$(\bar{1}00)$	1051.23
(010)	792.87
$(0\bar{1}0)$	604.16
(001)	666.53
$(00\bar{1})$	661.62

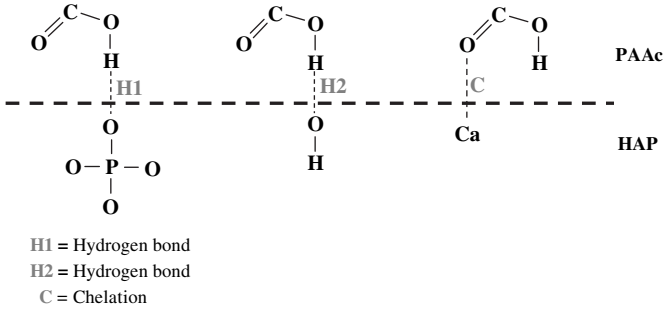

Fig. 10. Schematic representation of the formation of hydrogen bond and chelation. The notations used to represent hydrogen bond and chelation in Table 7 are shown.

Table 7
Hydrogen bond and chelation formation by different carboxylate groups of PAAc with different surfaces of HAP

	(100) surface	($\bar{1}$00) surface	(010) surface	(0$\bar{1}$0) surface	(001) surface	(00$\bar{1}$) surface
1st monomer					H1, C	
2nd monomer	H1, C				H1, C	
3rd monomer	H2, C					
4th monomer				H1, C		
5th monomer		H1, C	H1	H1		
6th monomer			C			
7th monomer		H1, C	H1, C	C		H1
8th monomer				H1		
9th monomer		H1, C	H1	H1	H1, C	H1, C
10th monomer	H1	H1	H1		H1, C	H1, C
11th monomer	H1, C	H1, C	H1	H1, C	H1	H1, C
12th monomer						
13th monomer	H1, C	H1	H1	C		H1
14th monomer	H1, C		H2	H1, C		

and chelation is shown in Fig. 10. Here, H1 is defined as the H-bond between surface oxygen atoms of PO_4^{-3} of HAP with hydrogen atoms of COOH group of PAAc, H2 is defined as the H-bond between oxygen atoms of OH^- of HAP with hydrogen atoms of COOH group of PAAc, and C is the chelation between surface calcium atoms of HAP with carbonyl oxygen atoms of COOH group of PAAc.

All the analyzed surfaces (Table 7) have potential sites for H1 and C formation. As oxygen or hydrogen atoms of surface OH^- ion in HAP are favorable sites for H-bond formation with hydrogen or carbonyl oxygen atoms of COOH group of PAAc, however, after simulations we have observed that only one H2 has been formed for each of the surfaces (100) and (010). This has happened because the surface OH^- ions are partially shielded by calcium atoms, as shown in relaxed model in Figs. 6 and 7, which prevents them from forming H-bond. Also, for all the above mentioned cases, unidentate (chelation) is formed between surface calcium atoms and oxygen atoms of COOH group (Fig. 10). In the case of ex situ HAP composites with PAAc, the polymer chain will interact with (001) or (00$\bar{1}$) surface of HAP as discussed earlier. The hydrogen bond formation is shown in Table 5, where all the hydrogen bonds are formed between oxygen atom of PO_4^{-3} and hydrogen atom of COOH group (H1). Hydrogen bond is not observed in these surfaces involving OH^- ions of HAP (H2). This results because on these surfaces, COOH groups first come across oxygen atoms of PO_4^{-3} and/or calcium atoms, and due to this, they form H-bond and/or chelation (unidentate) with these surface atoms and become unable to come close to OH^- ions for H-bond formation.

As it is discussed above all the surfaces, which were studied, have potential sites for H-bond and chelation (unidentate) formation which shows that significant interactions take place between HAP and PAAc, and carboxylate groups play a major role in these interactions as COOH is responsible for H-bond and/or chelation formation. Thus it appears that these composites have improved interface properties.

6. Conclusions

In this work, we have evaluated parameters of HAP in CVFF from a known potential function. Using these parameters both the obtained structure and also the vibrational spectra after MD simulations agree well with experiments. Using the obtained parameters of HAP and available parameters of PAAc in CVFF, an interaction study was performed. Binding energy calculations showed that there are preferred surfaces for PAAc attachment if all the surfaces investigated are indeed available. From these simulations, it appears that during in situ HAP preparation, there are some preferred surfaces which will form first. Also it can be inferred from these preferred surfaces that the *c*-axis of HAP aligns parallel to polymer chains with (100) surface is being most likely the one to form first. In ex situ HAP composites with PAAc, the binding energy is less as compared to surface (100). It was also observed that there were potential sites for H-bond and chelation formation, depending upon the surface. It was observed that surface OH^- ions in (001) surface do not form any H-bond with PAAc, but some surface OH^- ions in (100) and (010) surfaces do form H-bond with PAAc. The results obtained here show that interactions between HAP and PAAc are significant. Also, interactions in in situ HAP are more significant in comparison to ex situ HAP composites.

Evaluation of the nature of interactions at mineral–polymer interfaces is significant due to large impact of these interactions on overall mechanical behavior of the composite biomaterial. In composite systems, especially nanocomposite systems, interfaces may have significant role on mechanical properties [7,8,10]. Our simulations indicate that there are significant interactions at mineral–polymer interface which are due to functional group present in polymer and can be further modified by taking polymer with specific functional groups. Modification of these interfaces is particularly relevant for the designing of new biomaterial systems. As a result of this work, force field parameters are available for HAP in a commonly used CVFF. The CVFF is commonly used for the study of many polymers and biopolymers. Using the parameters described in this work, interactions of many polymers and biopolymers with HAP may be investigated for the designing of new biomaterials.

Acknowledgments

This research is partially funded by grant from National Science Foundation (CAREER # 0132768). The Cognizant program managers are Drs. Jorn Larsen-Basse and Yip-Wah Chung. Computations were performed on the SGI Onyx 300 with the IRIX 6.5.22 operating system of North Dakota BRIN (Biomedical Research Infrastructure Network) and SGI Origin (version 4.2 MS) of NCSA (National Center of Superconducting applications), at UIUC (University of Illinois at Urbana-Champaign).

References

[1] Aoki H. Medical applications of hydroxyapatite, vol. 1. Ishiyaku Euro-America; 1994. p. 156.
[2] Kikuchi M, Ikoma T, Itoh S, Matsumoto HN, Koyama Y, Takakuda K, et al. Compos Sci Technol 2004;64:819.
[3] Thorwarth M, Schulze-Mosgau S, Wehrhan F, Srour S, Wiltfang J, Neukan FW, et al. Biochem Biophys Res Commun 2005;329:789.
[4] Qian JJ, Bhatnagar RS. J Biomed Mater Res 1996;31:545.
[5] Itoh S, Kikuchi M, Koyama Y, Takakuda K, Shinomiya K, Tanaka J. Biomaterials 2002;23:3919.
[6] Murugan R, Ramakrishna S. Compos Sci Technol 2005;65:2385.
[7] Katti KS. Colloids Surf B 2004;39:133.
[8] Katti KS, Turlapati PK, Verma D, Gujjula PK, Katti DR. Am J Biochem Biotechnol 2006;2:73.
[9] Bhowmik R, Katti KS, Katti DR, Verma D. Mater. Sci. Eng C, in press.
[10] Katti KS, Gujjula P. In: Fifteenth ASCE engineering mechanics conference. New York, NY; 2002.
[11] Verma D, Katti KS, Katti DR. J Biomed Mater Res A 2006;77:59.
[12] Verma D, Katti KS, Katti DR. J Biomed Mater Res A 2006;78:772.
[13] Fermeglia M, Ferrone M, Pricl S. Mol Simul 2004;30:289.
[14] Minisini B, Tsobnang F. Compos Part A 2005;36:531.
[15] Shevade AV, Ryan MA, Homer ML, Manfreda AM, Zhou H, Manatt KS. Sens Actuators B 2003;93:84.
[16] Fermeglia M, Ferrone M, Pricl S. Fluid Phase Equilib 2003;212:315.
[17] Gardebien F, Gaudel-Siri A, Jean-Luc Brédas, Lazzaroni R. J Phys Chem B 2004;108:10678.
[18] Maple JR, Hwang MJ, Stockfisch TP, Dinur U, Waldman M, Ewig CS, et al. J Comput Chem 1994;15:162.
[19] Hwang M, Stockfisch TP, Hagler AT. J Am Chem Soc 1994;116:2515.
[20] Hagler AT, Ewig CS. Comput Phys Commun 1994;84:131.
[21] Dauber-Osguthorpe P, Roberts VA, Osguthorpe DJ, Wolff J, Genest M, Hagler AT. Proteins Struct Funct Genet 1988;4:31.
[22] Maple J, Dinur U, Hagler AT. Proc Natl Acad Sci USA 1988;85:5350.
[23] Shi S, Yan L, Yang Y, Fisher J. ESFF forcefield project report II. MSI, San Diego; 1998.
[24] Weiner SJ, Kollman PA, Case DA, Singh UC, Ghio C, Alagona G, et al. J Am Chem Soc 1984;106:765.
[25] Weiner SJ, Kollman PA, Nguyen DT, Case DA. J Comput Chem 1986;7:230.
[26] Brooks BR, Bruccoleri RE, Olafson BD, States DJ, Swaminathan S, Karplus M. J Comput Chem 1983;4:187.
[27] Momany FA, Rone R. J Comput Chem 1992;13:888.
[28] Jorgensen WL, Maxwell DS, Tirado-Rives J. J Am Chem Soc 1996;118:11225.
[29] Arnaud P, Zakrzewska K, Meunier B. J Comput Chem 2003;24:797.
[30] Stote RH, Karplus M. Proteins Struct Funct Genet 1995;23:12.
[31] Hori K, Kushick JN, Weinstein H. Biopolymers 1988;27:1865.
[32] Donini O, Weaver DF. J Comput Chem 1998;19:1515.
[33] Duffy EM, Kowalczyk PJ, Jorgensen WL. J Am Chem Soc 1993;115:9271.
[34] Katti DR, Schmidt S, Ghosh P, Katti KS. Clays Clay Miner 2005;53:171.
[35] Schmidt S, Katti DR, Ghosh P, Katti KS. Langmuir 2005;21:8069.
[36] Katti DR, Ghosh P, Schmidt S, Katti KS. Biomacromolecules 2005;6:3276.
[37] Teppen BJ, Rasmussen K, Bertsch PM, Miller DM, Schäfer L. J Phys Chem B 1997;101:1579.
[38] Hauptmann S, Dufner H, Brickmann J, Kast SM, Berry RS. Phys Chem Chem Phys 2003;5:63.
[39] de Leeuw NH. Phys Chem Chem Phys 2004;6:1860.
[40] Lee WT, Dove MT, Salje EKH. J Phys Condens Matter 2000;12:9829.
[41] Zahn D, Hochrein O. Phys Chem Chem Phys 2003;5:4004.
[42] de Leeuw NH. J Phys Chem B 2004;108:1809.
[43] Zahn D, Hochrein O. Z Anorg Allg Chem 2005;631:1134.
[44] Hochrein O, Kniep R, Zahn D. Chem Mater 2005;17:1978.
[45] Kleinhesselink D, Wolfsberg M. Surf Sci 1992;262:189.
[46] Allen MP, Tildesley DJ. Computer simulation of liquids. New York: Oxford University Press; 1987.
[47] Hollas JM. Modern spectroscopy. 3rd ed. New York: John Wiley & Sons; 1996.
[48] Suzuki S, Kawamura K. J Phys Chem B 2004;108:13468.
[49] Eyring H, Walter J, Kimball GE. Quantum chemistry. New York: John Wiley; 1944.
[50] Force-field based simulation documentation. San Diego, CA: Accelrys Software Inc.
[51] Elliot JC, Mackie PE, Young RA. Science 1973;180:1055.
[52] Fumi FG, Tosi MP. J Phys Chem Solids 1964;25:31.
[53] Fumi FG, Tosi MP. J Phys Chem Solids 1964;25:45.
[54] Yuen PS, Murfitt RM, Collin RL. J Chem Phys 1974;61:2383.
[55] Ritschla F, Faitb M, Fiedlera K, JKöhlerc JEH, Kubiasb B, Meisela M. Z Anorg Allg Chem 2002;628:1385.
[56] Suetsugu Y, Tanaka J. J Mater Sci Mater Med 2002;13:767.
[57] Ignjatovic N, Savic V, Najman S, Plavsic M, Uskokovic D. Biomaterials 2001;22:571.
[58] Ikoma T, Yamazaki A, Nakamura S, Akao M. J Solid State Chem 1999;144:272.
[59] Karasawa N, Goddard III WA. J Phys Chem 1989;93:7320.
[60] Andersen HC. J Chem Phys 1980;72:2384.
[61] Taylor D. Trans Br Ceram Soc 1988;87:88.
[62] de Leeuw NH. Phys Chem Chem Phys 2002;4:3865.
[63] Bertaut FCR. Acad Sci. Paris 1958;246:3447.
[64] Tasker PW. J Phys C Solid State Phys 1979;12:4977.
[65] Singh UC, Kollman PA. J Comput Chem 1984;5:129.
[66] Frisch MJ, Trucks GW, Schlegel HB, Scuseria GE, Robb MA, Cheeseman JR, et al. Gaussian 03. Pittsburgh PA: Gaussian, Inc; 2003.
[67] Smith GD, Jaffe RL, Yoon DY. J Phys Chem 1993;97:12752.
[68] Tanaka G, Goettler LA. Polymer 2002;43:541.
[69] Gardebien F, Bredas Jean-Luc, Lazzaroni R. J Phys Chem B 2005;109:12287.
[70] Mkhonto D, de Leeuw NH. J Mater Chem. 2002;12:2633.
[71] Deer WA, Howie RA, Zussman J. An introduction to the rock-forming minerals. Longman, UK; 1992.